Bulletin of the Seismological Society of America, Vol. 81, No. 6, pp. 2234–2253, December 1991

DIFFRACTION OF *P*, *SV*, AND RAYLEIGH WAVES BY TOPOGRAPHIC FEATURES: A BOUNDARY INTEGRAL FORMULATION

By Francisco J. Sánchez-Sesma and Michel Campillo

Abstract

A method is presented to compute the diffraction of *P*, *SV*, and Rayleigh waves by an irregular topographic feature in an elastic half-space. It is based on an integral representation of the diffracted elastic fields in terms of single-layer boundary sources that is derived from Somigliana's identity. Introduction of boundary conditions leads to a Fredholm integral equation of the second kind for boundary sources. A discretization scheme based on the numerical and analytical integration of exact Green's functions for displacements and tractions is employed. Calculations are performed in the frequency domain and synthetic seismograms are obtained using the fast Fourier transform.

In order to give perspective on the range of effects caused by topographic anomalies, various examples that cover extreme cases are presented. It is found that topography may cause significant effects both of amplification and of deamplification at the irregular feature itself and its neighborhood, but the absolute level of amplification is generally lower than about four times the amplitude of incoming waves. Such facts must be taken into account when the spectral ratio technique is used to characterize topographical effects.

Introduction

Site effects can generate large ground motion amplification during earthquakes. This fact is well known (see, e.g., Sánchez-Sesma, 1987, and Aki, 1988, for recent reviews). However, quantitative procedures to account for topographical amplification in practical instances are less well known. According to Geli *et al.* (1988), observed amplification values in the field are systematically larger than theoretical predictions based on scalar two-dimensional models. They have pointed out the need to study the effects that the propagation of *P*, *SV*, and Rayleigh waves may produce at and near irregular two- and three-dimensional configurations in order to better explain the observations.

The problem is not new. Significant progress has been achieved since the pioneering work of Aki and Larner (1970), who introduced a numerical method based on a discrete superposition of plane waves. At the same time, Trifunac (1971, 1973) found the analytical solutions for the response of semi-circular alluvial valleys and canyons under incident *SH* waves. For arbitrary geometries, a formulation based on an integral representation was used by Wong and Jennings (1975). On the other hand, Bouchon (1973) and later Bard (1982) and Geli *et al.* (1988) used the Aki–Larner technique to study the response of irregular topographies. This method, however, cannot deal with large slope features because of the numerical difficulties to correctly simulate locally upgoing waves (see Sánchez-Sesma *et al.*, 1989, for a discussion). In practice, this problem has been removed by using the combination of boundary integral representations with the discrete wavenumber method. Bouchon (1985), Campillo and Bouchon (1985), Campillo (1987), Gaffet and Bouchon (1989), Bouchon *et al.* (1989), and Campillo *et al.* (1990) used direct source distribu-

tions on the boundaries, whereas Kawase (1988) and Kawase and Aki (1989) used Somigliana representation (see, e.g., Aki and Richards, 1980).

Another type of boundary method has been used to deal with this class of problems (see, e.g., Sánchez-Sesma, 1978; Sánchez-Sesma and Rosenblueth, 1979; Sánchez-Sesma and Esquivel, 1979; Wong, 1979, 1982; Dravinski, 1982; Dravinski and Mossessian, 1987; Sánchez-Sesma *et al.*, 1985; Bravo *et al.*, 1988; Eshraghi and Dravinski, 1989; Khair *et al.*, 1989; Bouden *et al.*, 1990; Luco *et al.*, 1990). In its many variants, including in some cases three-dimensional problems and layered media, the technique is based upon the superposition of solutions for sources with their singularities placed *outside* the region of interest. Boundary conditions are satisfied in a least-squares sense (Wong, 1982, considered the problem as one of generalized inversion). This leads to a system of linear equations for the sources' strengths. In some applications, however, the location of sources requires particular care and the trial and error process needed is difficult to apply. This is particularly true when many frequencies are to be computed.

In this work, we use a single-layer boundary integral representation for diffracted waves. In this respect, this approach is similar to the *source* method just mentioned above, except for the fact that now we put the sources at the boundary and directly solve the linear system that arise from the discretization. In this way, the uncertainty about the location of sources is eliminated. This approach was motivated by the success achieved using the combination of boundary integral formulations and the discrete wave number method (e.g., Bouchon, 1985; Campillo and Bouchon, 1985; Campillo, 1987; Kawase, 1988; Kawase and Aki, 1989). Such a combination is particularly attractive as the singularities of Green's functions are not present in each one of the terms of the discrete wave number expansion. The integration along the boundary effectively makes the singularities vanish and improves convergence as well. However, such procedures require considerable amount of computer resources. For many applications, an alternative approach may be welcomed. Indeed, when the Green's functions are explicit, its singularities are integrable as it is done in numerous BIEM applications (see, e.g., Brebbia, 1978; Banerjee and Butterfield, 1981). In fact, our direct approach retains the physical insight of the source method, with all the benefits of analytical integration of *exact* Green's functions. We represent diffracted fields with the superposition of the radiation from boundary line sources computed using the exact expressions of the two-dimensional Green's functions in an unbounded elastic space.

In what follows, we show that a direct single-layer boundary integral representation stems from that of Somigliana, and we apply it to study the surface motion at various topographic features for incident P, SV, and Rayleigh waves. This plane strain case can be regarded as the simplest of a class of vector problems of seismological interest.

In order to test our method, we compared results with those obtained by Wong (1982), Sánchez-Sesma *et al.* (1985), and Kawase (1988) for the diffraction of P, SV, and Rayleigh waves by a semicircular canyon on a half-space. We found excellent agreement with these results. Various examples that cover extreme profiles are presented. Thus, giving perspective on the range of effects caused by topography, we show that relatively simple topographies may induce significant variations of ground-motion at and around the irregularity. We believe that this fact explains the large relative amplifications reported in the literature (see,

e.g., Geli *et al.*, 1988). Our examples show that, even though relative amplification due to the topography is sometimes quite big, the absolute level of amplification is generally lower than about four times the amplitude of incoming waves. Such facts must be taken into account when the spectral ratio technique is used to characterize topographical effects.

Integral Representation Using Boundary Sources

Consider the domain V and its boundary S. If an elastic material occupies such a region, the displacement field under harmonic excitation can be written by means of the Somigliana representation theorem for an interior problem (see, e.g., Achenbach, 1973; Aki and Richards, 1980; Banerjee and Butterfield, 1981):

$$cu_m(\xi) = \int_S \left[G_{im}(\mathbf{x}, \xi) t_i(\mathbf{x}) - T_{im}(\mathbf{x}, \xi) u_i(\mathbf{x}) \right] dS_{\mathbf{x}} + \int_V f_i(\mathbf{y}) G_{im}(\mathbf{y}, \xi)\, dV_{\mathbf{y}}, \tag{1}$$

where u_m = mth component of displacement; t_i = ith component of traction at the boundary; $G_{im}(\mathbf{x}, \xi)$ = Green function, i.e., the displacement in the direction i at point $\mathbf{x}$ due to the application of a unit force in the direction m at point ξ; $T_{im}(\mathbf{x}, \xi)$ = traction Green function, i.e., the traction in the direction i at point $\mathbf{x}$ on the boundary with normal $\mathbf{n}(\mathbf{x})$ (assumed to be specified) due to the application of a unit force in the direction m applied at ξ; and f_i = components of body force distribution. The constant c takes the values 1 or 0 if the point ξ is inside or outside V, respectively, and is equal to 0.5 when ξ is located on the smooth boundary. The subscripts in the differentials indicate the space variable over which the integration is performed. This representation theorem is the departure of various integral formulations and seismological applications (see, e.g., Aki and Richards, 1980).

Assume now that $u'_i(\mathbf{x})$ is a solution of the exterior problem with boundary traction $t'_i(\mathbf{x})$. Assume also that the material that occupies the exterior region is the same. Therefore, both interior and exterior regions share Green's functions. Neglecting body forces we can write

$$c' u'_m(\xi) = -\int_S \left[G_{im}(\mathbf{x}, \xi) t'_i(\mathbf{x}) - T_{im}(\mathbf{x}, \xi) u'_i(\mathbf{x}) \right] dS_{\mathbf{x}}, \tag{2}$$

where c' is a constant with values 0, 0.5, or 1 if the point ξ is inside V, at S, or outside V, respectively. In writing equation (2), the radiation conditions at infinity of the displacement fields have been taken into account.

Summing up equations (1) and (2), we have

$$cu_m + c' u'_m = \int_S \left[(t_i - t'_i) G_{im} - (u_i - u'_i) T_{im} \right] dS_{\mathbf{x}} + \int_V f_i G_{im}\, dV_{\mathbf{y}}. \tag{3}$$

If we impose that at the boundary $u_i = u'_i$ and if $t_i - t'_i = \phi_i$ we can write

$$u_m(\xi) = \int_S \phi_i(\mathbf{x}) G_{im}(\mathbf{x}, \xi)\, dS_{\mathbf{x}} + \int_V f_i(\mathbf{y}) G_{im}(\mathbf{y}, \xi)\, dV_{\mathbf{y}}, \tag{4}$$

which is a representation valid in region V and its boundary S. On the other hand, the Green function satisfies

$$G_{im}(\mathbf{x}, \xi) = G_{mi}(\mathbf{x}, \xi) = G_{mi}(\xi, \mathbf{x}); \tag{5}$$

therefore, we can write

$$u_i(\mathbf{x}) = \int_S \phi_j(\xi) G_{ij}(\mathbf{x}, \xi)\, dS_\xi + \int_V f_j(\xi) G_{ij}(\mathbf{x}, \xi)\, dV_\xi, \tag{6}$$

where $\phi_j dS_\xi$ is clearly a force distribution at the boundary. This *single layer* integral representation has been studied by Kupradze (1963). He showed that the displacement field is continuous across S if $\phi_j(\xi)$ is continuous on S. This is in agreement with our choice for $u_i = u'_i$. Other choices are possible. If for example $t'_i = t_i$, then $u_i - u'_i$ would be unknown and the displacement field would be expressed in terms of the *traction* Green's function. (This is an usual approach in dealing with certain crack problems; see, e.g., Bonnet, 1989; Coutant, 1989). With our derivation, that closely follows that of Bonnet (1986a), we have shown that this *single layer* integral representation stems from Somigliana's one. In its scalar version (*SH* waves), it is called the Kirchhoff–Helmholtz representation (see, e.g., Kouoh-Bille *et al.*, 1991).

This integral representation allows computation of stresses and tractions by direct application of Hooke's law. However, when $\mathbf{x} = \xi$ on the boundary, this requires particular care. From a limiting process based on equilibrium considerations around an internal neighborhood of the boundary, we can write, for $\mathbf{x}$ on S that

$$t_i(\mathbf{x}) = \frac{1}{2}\phi_i(\mathbf{x}) + \int_S \phi_j(\xi) T_{ij}(\mathbf{x}, \xi)\, dS_\xi + \int_V f_j(\xi) T_{ij}(\mathbf{x}, \xi)\, dV_\xi. \tag{7}$$

The first term of the right hand side must be dropped if $\mathbf{x}$ is inside V. This result has also been found by Kupradze (1963). He used a formal technique of singularity extraction that is now used to deal with the hypersingular integral equations of dynamic elasticity (see, e.g., Bonnet, 1986b, 1989).

Equations (6) and (7) are the basis of our approach. They allow direct interpretation of all physical quantities involved.

Two-Dimensional Green's Functions in Unbounded Space

In a homogeneous isotropic elastic unbounded medium, the Green functions for harmonic time dependence $e^{i\omega t}$, where $i^2 = -1$, ω = circular frequency, and

t = time, can be expressed in the following compact form:

$$G_{22} = \frac{1}{i4\rho}\,\frac{H_0^{(2)}(kr)}{\beta^2},$$

$$G_{ij} = \frac{1}{i8\rho}\left[\delta_{ij}A - (2\gamma_i\gamma_j - \delta_{ij})B\right] \quad i,j = 1,3, \tag{8}$$

$$T_{22} = \frac{i}{4r}\,D(kr)\gamma_k n_k,$$

$$T_{ij} = \frac{i\mu}{2\rho r}\left\{\left[B + \frac{\lambda D(qr)}{2\mu\alpha^2}\right]\gamma_j n_i + \left[B + \frac{D(kr)}{2\beta^2}\right] \times\left[\gamma_i n_j + \gamma_k n_k \delta_{ij}\right] + (C - 4B)\gamma_i\gamma_j\gamma_k n_k\right\},$$

where

$$A = \frac{H_0^{(2)}(qr)}{\alpha^2} + \frac{H_0^{(2)}(kr)}{\beta^2},$$

$$B = \frac{H_2^{(2)}(qr)}{\alpha^2} - \frac{H_2^{(2)}(kr)}{\beta^2}, \tag{9}$$

$$C = \frac{D(qr)}{\alpha^2} - \frac{D(kr)}{\beta^2},$$

$$D(p) = pH_1^{(2)}(p),$$

ρ = mass density, $k = \omega/\beta = S$ wavenumber, $q = \omega/\alpha = P$ wavenumber, $\alpha = \sqrt{(\lambda + 2\mu)/\rho}$ = P-wave velocity, $\beta = \sqrt{\mu/\rho}$ = S-wave velocity, λ, μ = Lamé's constants, δ_{ij} = Kronecker's delta, $\gamma_j = (x_j - \xi_j)/r$, n_j = unit normal vector, $r = \sqrt{(x_1 - \xi_1)^2 + (x_3 - \xi_3)^2}$, and $H_m^{(2)}(.)$ = Hankel function of the second kind and order m.

In the previous expressions, the usual summation convention for subscripts is assumed and it is restricted to 1 and 3 because of the two-dimensional nature of the problem considered herein, i.e., there is no dependence to x_2. We may use in what follows the usual correspondence for axis' names: $x_1 = x$, $x_2 = y$, and $x_3 = z$, respectively. Also: $u_1 = u_x = u$ and $u_3 = u_z = w$. The terms G_{22} and T_{22} correspond to a *SH antiplane* unit line force, whereas G_{ij} and T_{ij}, where i, $j = 1, 3$, are associated to an *inplane* unit line force with direction j. Terms G_{2j}, G_{j2}, T_{2j}, and T_{j2} are null for $j = 1, 3$. Similar expressions for the in-plane Green's functions have been presented by Kummer *et al.* (1987).

Equations (8) and (9) allow a direct view of their singularities at the point of application of the line force. The singularity of displacements is logarithmic. This can be seen from the behavior of Hankel functions for small arguments (see, e.g., Abramowitz and Stegun, 1972). Regarding the tractions, the singularity is explicitly of the form r^{-1} because for zero arguments we have the constant limiting forms: $D = 2i/\pi$ and $C = 2B = 2i(\alpha^{-2} - \beta^{-2})/\pi$. In particular, when frequency tends to zero, equations (8) lead to their static counterparts

(see, e.g., Love, 1944). These properties are invoked below in connection with our discretization scheme.

Diffraction of Elastic Waves by a Topographic Feature

Consider an elastic half space with a localized topographic relief as depicted in Figure 1. The ground motion in this irregular configuration comes from the interferences of incoming waves with reflected and diffracted ones. It is also usual to say that the total motion is the superposition of the so called *diffracted* waves and the free-field:

$$u_i = u_i^{(0)} + u_i^{(d)}, \tag{10}$$

where $u_i^{(0)}$ = free-field displacement, i.e., the solution in the absence of the irregularity. In this application, the displacement free-field is that produced by incident plane waves and is analytically extended to the parts of topography that are not included in the reference half-space. This means that incoming and reflected waves are assumed to exist for $z < 0$ fulfilling the *same* analytical expressions that they satisfy for $z \geqq 0$. Therefore, the free-field is continuous everywhere.

According to our previous discussion, the diffracted field is given by equation (6), which, in the absence of body forces, can be written as

$$u_i^{(d)}(\mathbf{x}) = \int_S \phi_j(\xi) G_{ij}(\mathbf{x}, \xi)\, dS_\xi. \tag{11}$$

The traction-free boundary condition implies that $t_i^{(0)} + t_i^{(d)} = 0$. Then, from equation (7) such condition can be expressed by means of

$$\frac{1}{2}\delta_{ij}\phi_j(\mathbf{x}) + \int_S \phi_j(\xi) T_{ij}(\mathbf{x}, \xi)\, dS_\xi = -t_i^{(0)}(\mathbf{x}), \tag{12}$$

which is a singular Fredholm integral equation of the second kind for the boundary sources, i.e., those producing the diffracted field. This expression is discretized along a finite portion of the boundary S that includes the topography and the lateral flat parts. We have used values of $3L$ to $5L$, where

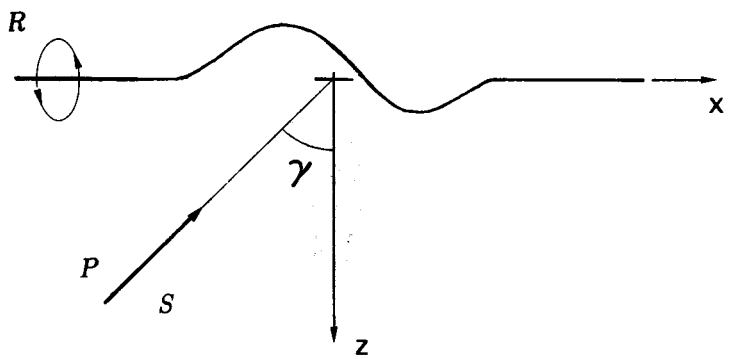

Fig. 1. Irregular half-space and incidence of plane P, SV, and Rayleigh waves.

L = surface length of the surface anomaly. Assuming $\phi_j(\xi)$ constant over each of the N boundary segments with equal length ΔS leads to the system of linear equations

$$\sum_{l=1}^{N} \phi_j(\xi_l)\mathbf{t}_{ij}(\mathbf{x}_n, \xi_l) = -t_i^{(0)}(\mathbf{x}_n), \quad n = 1, N, \tag{13}$$

where

$$\mathbf{t}_{ij}(\mathbf{x}_n, \xi_l) = \frac{1}{2}\delta_{ij}\xi_{nl} + \int_{\xi_l - \frac{\Delta S}{2}}^{\xi_l + \frac{\Delta S}{2}} T_{ij}(\mathbf{x}_n, \xi)\, dS_\xi. \tag{14}$$

These integrals are computed numerically using Gaussian integration except when $n = l$. In this case, we have

$$\mathbf{t}_{ij}(\mathbf{x}_n, \xi_n) = \frac{1}{2}\delta_{ij}, \tag{15}$$

because the integral in equation (14) for $n = l$ is null as long as the discretization segment is a straight line, which is the case assumed here. From equations (8), it can be verified that, under this circumstance, the integrand is a singular *odd* function on the segment. Therefore, its Cauchy's principal value is zero. The value for $\mathbf{t}_{ij}$ in equation (15) can be interpreted as half of the applied unit line force and means that the force is distributed symmetrically for any two half-spaces containing the line of application of the load, regardless of its direction. In fact, this result also corresponds to the static solution.

Once the values of $\phi_j(\xi_l)$ are known, the diffracted field is computed by means of

$$u_i^{(d)}(\mathbf{x}) = \sum_{l=1}^{N} \phi_j(\xi_l)\mathbf{g}_{ij}(\mathbf{x}, \xi_l), \tag{16}$$

where

$$\mathbf{g}_{ij}(\mathbf{x}, \xi_l) = \int_{\xi_l - \frac{\Delta S}{2}}^{\xi_l + \frac{\Delta S}{2}} G_{ij}(\mathbf{x}, \xi)\, dS_\xi. \tag{17}$$

These integrals are also computed numerically with Gaussian integration, except in the case when $\mathbf{x}$ is in the neighborhood of ξ_l, for which we obtained analytical expressions from the ascending series for Bessel functions (see, e.g., Abramowitz and Stegun, 1972). For example, the integral of the Hankel function

$$\int_{-\Delta S/2}^{\Delta S/2} H_0^{(2)}(k\,|\,s\,|)\, ds$$

can be written as $\Delta S[1 + i2/\pi(1 - \gamma - \log k\Delta S/4)]$, where γ = Euler constant, if only the leading terms of the series are taken. We considered up to quadratic

terms, which is enough if the number of segments per wavelength is larger than about 6.

For the elevated portions of the relief, the analytical extension of the free-field provides the boundary excitation. In the case of incident Rayleigh waves or for SV waves with incidence angle larger than the critical one, the analytical extension gives exponential growth of the extended field (incident plane SV waves with an incident angle of 45°, having no mode conversion and unit reflection coefficient, do not present this effect). This difficulty, when it appears, can be solved by means of an adaptative integration scheme, but it implies heavy computation. One way to remove this problem is to define an auxiliary region limited by the irregular topography and a fictitious boundary completely embedded in the half-space. The corresponding integral equation and the conditions of continuity of displacements and tractions may lead to the solution (see, e.g., Kawase and Aki, 1990). Obviously, in that case there is no need of the analytical extension. However, as we desire to keep only one region, we choose to produce Rayleigh waves by loading our irregular half-space with a vertical force. Then, the excitation comes from imposing vertical tractions in a small region of the flat part of the free surface. This is an *ad hoc* solution to the problem and illustrates well the wide potential applications of our method. In fact, the surface load problem is well known (Lamb, 1904). In this case, more of two thirds of the total energy is radiated as Rayleigh waves (Woods, 1968). Regarding our application, at the surface the relative amount of Rayleigh waves is much larger.

Testing of the Method and Discussion

The accuracy of this approach has been gauged by comparing results with those obtained by Wong (1979, 1982), Sánchez-Sesma *et al.* (1985), and Kawase (1988). The diffraction of P, SV, and Rayleigh waves by a semi-circular canyon has been studied by Wong (1979, 1982) for a half-space with Poisson ratio of 1/3 and no attenuation using a boundary method.

Wong's results (1982) were verified by Sánchez-Sesma *et al.* (1985) and Dravinski and Mossessian (1987) for a normalized frequency $\eta = \omega a / \pi \beta = 0.5$, where a is the radius of the canyon. Generally excellent agreement was found for incident P and SV waves.

For a larger normalized frequency $\eta = 2$, results by Wong (1982) and Kawase (1988) are available for P and SV waves with 0 and 30 degrees of incidence angle each. Kawase (1988) used a boundary integral representation combined with the discrete wavenumber method. Figures 2 and 3 display our results for both horizontal and vertical displacement amplitudes with solid and dashed lines, respectively. We considered a total discretization length of $5L$, where $L = \pi a$ and 15 segments per S wavelength. The solution is stable even when such parameters are reduced to $3L$ and to 6, respectively. Wong's and Kawase's results are shown by symbols. Excellent agreement is found for both horizontal and vertical components. However, small differences can be seen among these results. For instance, both Wong (1982) and Kawase (1988) predict amplitudes at the "incidence" rim of the canyon that are somewhat larger than our results for SV incidence with 30° (Fig. 3b). Generally, our results (see also Figs. 2 and 3) are closer to those of Kawase. However, in some cases they approach those of Wong. For some locations, both inside and outside the canyon our results are in between.

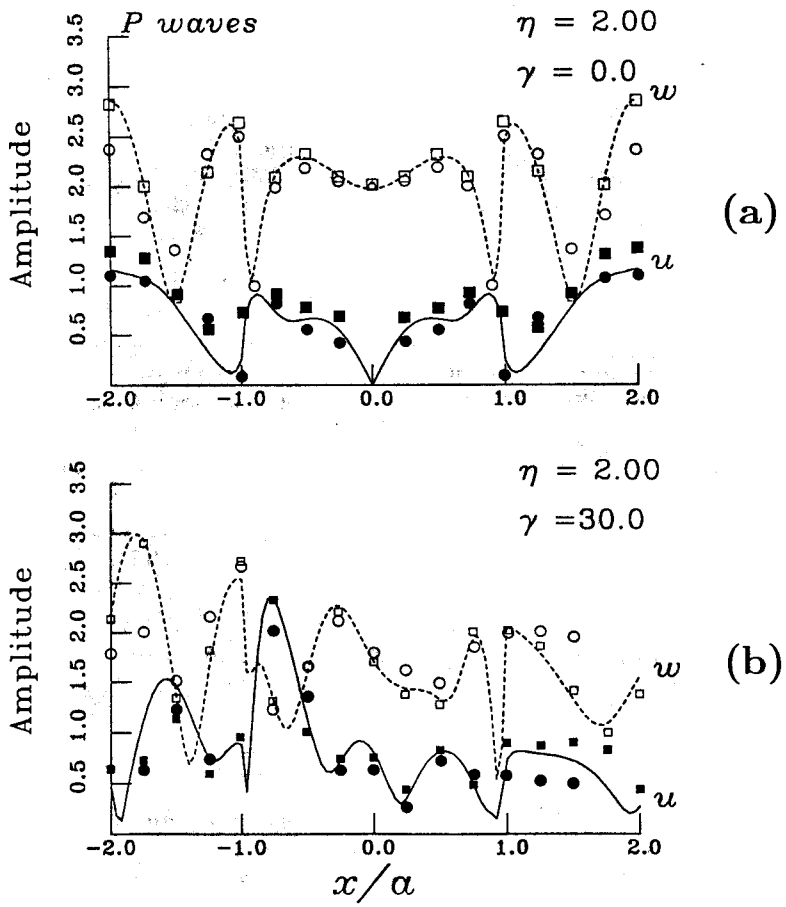

FIG. 2. Amplitudes of horizontal and vertical displacements for incidence of harmonic P waves upon a semicircular canyon; (a) vertical incidence, (b) 30° incidence. Poisson ratio is 1/3 and the normalized frequency $\eta = 2$. Solid and dashed lines correspond to horizontal (u) and vertical (w) components obtained in the present study, while solid and open symbols correspond to previous works. The results by Wong (1982) and those by Kawase (1988) are represented by circles and squares, respectively.

These three methods are approximate. The only way to assess their accuracy is through comparisons of results among them and with other procedures and by comparing the assumptions and the characteristics of each one as well.

Both Wong (1982) and Kawase (1988) considered as departure Lamb's (1904) integrals for the half-space. Working directly in frequency domain, Wong (1982) computed such integrals with "4 digits of accuracy." He considered such solutions for compressional and shear line sources as trial functions with the singularities "removed from the domain of interest," i.e., *outside* the irregular half-space, inside the region left by the canyon. He satisfied boundary conditions using a generalized inversion scheme, which guarantees good results in a global sense. On the other hand, Kawase (1988) integrated analytically along the boundary the terms of the discrete wavenumber expansion for which he assumed a horizontal periodicity of 10 times the diameter of the canyon, then by careful monitoring he computed the appropriate summations to get the coeffi-

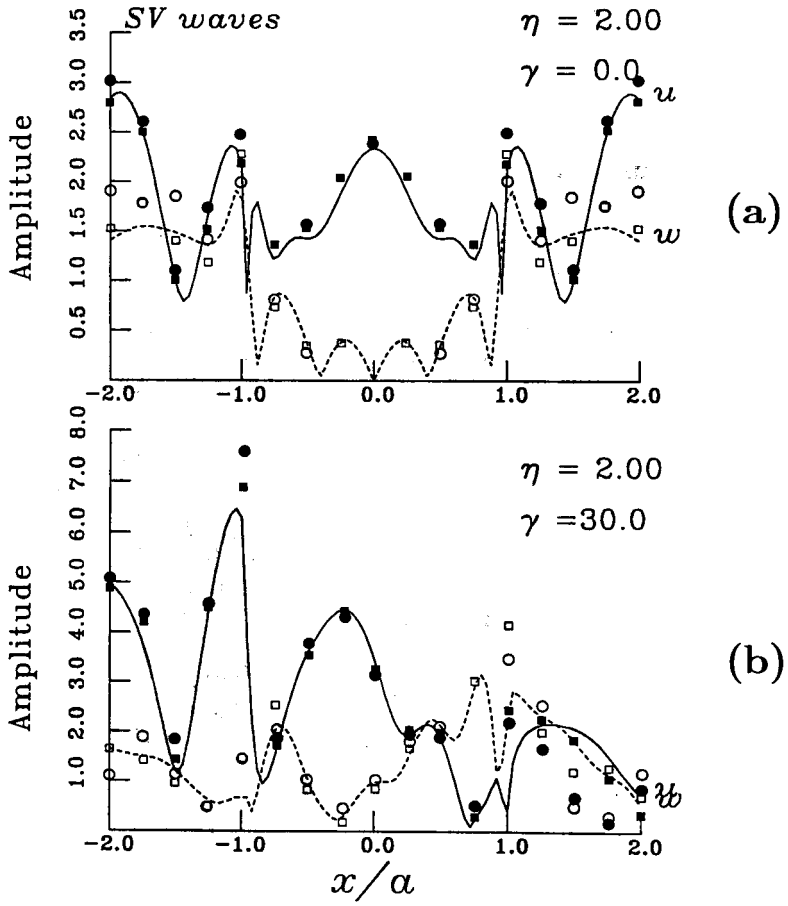

FIG. 3. Amplitudes of horizontal and vertical displacements for incidence of harmonic SV waves upon a semicircular canyon; (a) vertical incidence, (b) 30° incidence. The interpretation of the figure and parameters is the same as in Figure 2.

cients of the linear system of equations. He used an imaginary frequency to damp out the effect of the spurious sources introduced by the periodicity assumption. In order to obtain reliable results in the frequency domain, Kawase first got time series, then corrected with an exponentially increasing time window, which compensates for the effect of the imaginary frequency. Spectral ratios were then computed from the Fourier transforms of both the response and the input waveforms.

In contrast, we work directly in frequency domain and used the exact Green's function for the whole-space. Our approach is aimed to obtain diffracted waves, i.e., those produced both at the irregular boundary and at the free surface by means of the direct distribution of boundary sources for which we obtained either exact or analytical values at singularities. Hence, this formulation can be seen as an approximate numerical realization of Huygens' principle. For the numerical integration, we used Gaussian integration of three points per segment (which would produce exact results for a polynomial integrand of fifth degree; considering a typical value of six segments per S wavelength, our

numerical integrations can well be regarded as exact). To examine edge effects due to the finite size of the discretized boundary, we performed several tests and found that, for the range of frequencies studied, it suffices to discretize a total length of $3L$, where L = surface length of the topographic feature. The comparisons presented here have been computed for total discretization lengths of $3L$ and $5L$ and the results are virtually the same. It shows that edge effects have little or no influence in our computations and that, apart from the discretization of part of the free boundary, there is no need for fictitious or absorbing boundaries. We consider this fact a significant advantage of our approach. In order to qualitatively verify the validity of this interpretation, we computed the phase of diffracted waves and observed that for both components the phase variation with space shows slopes consistent with the expected outgoing nature of such waves. Figure 4 displays the phase of diffracted waves from the semi-circular canyon studied for incident P, SV (both with incidence angle of 30 degrees) and Rayleigh waves, respectively. It was assumed a normalized frequency of $\eta = 2$. Note that the slopes of the plots are negative (positive) for the positive (negative) portion of the flat boundary displayed. Therefore, our boundary sources correctly produce diffracted waves and their essentially *outgoing* characteristics.

Examples

In order to give some perspective on the range of effects caused by topography, various examples that cover extreme geometries are presented. We chose from a big set of results a sample that, being of reasonable dimension, allows one to describe the salient characteristics of such effects. Our results are displayed in both frequency and time domains for various canyons and mountains under incident, P, SV, and Rayleigh waves. A Poisson coefficient of 0.25 was selected and no attenuation was assumed. We considered four topographies: (1) a triangular canyon with a maximum depth of $\sqrt{3}a$ (dipping angles of 60°); (2) a semi-elliptical canyon with a maximum depth of three times the half width ($h = 3a$); (3) a triangular mountain with dipping angles of 45°; and (4) a semi-elliptical mountain with maximum height of $2a$. The discretization is extended over a total length of only 3 times the surface length of the topographic feature. The relatively small size of the discretized region is an advantage of the direct formulation. In the following examples, we used 15 segments per S wavelength.

For these topographies, we considered various cases of incidence of elastic waves. The incidence angles selected for P and SV waves were 30°, with respect to the vertical. For the canyons, the incident Rayleigh wave is a plane wave, whereas for the mountains such a pulse is generated with a vertical load of 12.5 force units applied over a length of $0.25a$ centered at $x = -4.5a$ for the semi-elliptical mountain and $x = -2.5a$ for the triangular one. These results are displayed on six figures (from Fig. 5 to Fig. 10). Each figure contains four plots: synthetic seismograms for horizontal and vertical components, respectively, frequency response for selected receivers, and spatial variation at a given frequency.

Computations were performed in the frequency domain and synthetic seismograms where computed using the FFT algorithm for a Ricker wavelet with central frequency $\omega_p = 1.5\pi\beta/a$ for 101 receivers equally spaced between $x = -4a$ and $x = 4a$ for the semi-elliptical profiles and between $x = -2a$ and

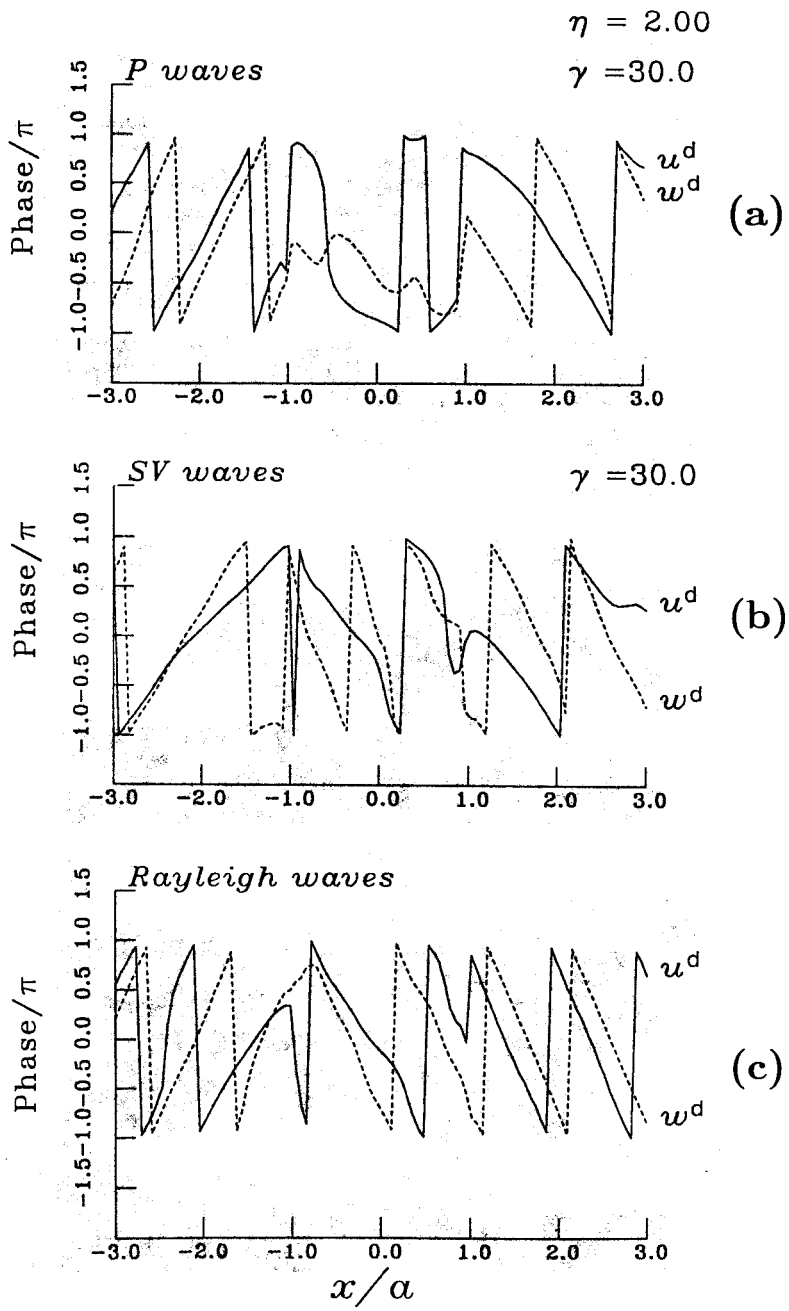

FIG. 4. Phases of horizontal and vertical diffracted displacements for incidence of harmonic waves upon a semicircular canyon; (a) P waves at 30° incidence, (b) SV waves at 30° incidence, and (c) Rayleigh waves. Solid and dashed lines correspond to horizontal ($u^{(d)}$) and vertical ($w^{(d)}$) components obtained in the present study. The parameters are the same as in Figure 2.

$x = 2a$ for the triangular ones. It was assumed that $2a/\beta = 1$ sec in order to define the time scale. For example, if $2a/\beta$ has another value, say 0.5, for $a = 0.5$ km and $\beta = 2$ km/sec, the time range will be half of the one used here; the actual time scale is then $\beta t/2a$.

Results in frequency domain are presented against $\omega a/\pi\beta$ and correspond to nine equally spaced surface receivers (out of the 101 for which we computed the synthetics). Our purpose is to give a view of the range of amplification and of its large variability rather than to present the individual response curves. In any case, we displayed also the amplitude of both horizontal and vertical displacements as a function of the receiver location for the frequency corresponding to the central one of the Ricker pulse.

For elevated topographies, the cases labeled "Rayleigh wave" correspond to the vertical load discussed above, and the frequency spectra clearly show the logarithmic singularity for the vertical displacement at small frequencies. In this case, the vertical displacement for a static load is also logarithmic in r (Love, 1944) and can have an arbitrary additive constant. Therefore, for the purpose of plotting the frequency dependence of displacement amplitude, the zero frequency values correspond to $\omega a/\pi\beta = 0.005$. However, both the synthetics and the results in the frequency domain, for $\omega a/\pi\beta > 1$ correctly describe the effects of topography upon incidence of Rayleigh waves. In fact, this can be seen on the synthetics, which show the appropriate amplitude of the incident Rayleigh wave.

Figure 5 displays the response of the triangular canyon for incident SV waves with incidence angle of 30°. Reflected P waves and diffracted Rayleigh waves can be identified on the synthetics for left and right parts of the

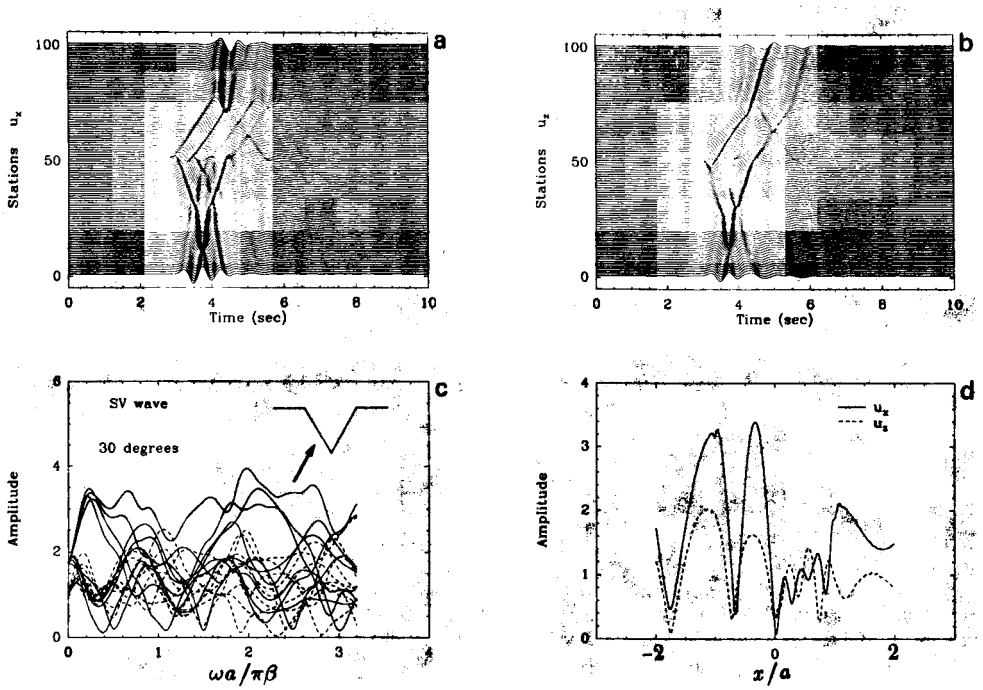

FIG. 5. Incidence of a plane SV wave with incidence angle of 30°. Synthetic seismograms and frequency response for surface receivers equally spaced between $x = -2a$ and $x = 2a$ at the surface of a triangular canyon with dipping angles of 60°. (a) and (b) horizontal and vertical components, u_x and u_z, respectively. The incident time signal is a Ricker wavelet with central frequency $\omega_p = 1.5\pi\beta/a$. Amplitudes of horizontal (continuous line) and vertical (dotted line) surface displacements (c) for nine receivers against normalized frequency and (d) for the central frequency of the Ricker wavelet for all the receivers against their horizontal location.

irregularity resulting in a criss-cross pattern and a significant increase of duration. The frequency domain results show large variations. For the horizontal component and for a wide range of frequencies, relative amplifications or deamplifications are larger than 20. However, maximum amplification is of about 4 times the amplitude of incoming wave in the horizontal component at the left rim. Note that frequency response for this point oscillates around the expected amplification (3.46 and 2 for horizontal and vertical motion, respectively) for an infinite wedge with internal angle of 120° and this incidence of SV waves (Sánchez-Sesma, 1990). Synthetic seismograms display this effect in the early response of left rim.

Figures 6 and 7 illustrate the surface motion of the deep semi-elliptical canyon for incident plane P and Rayleigh waves, respectively. Again, large variability emerges as a consequence of the superposition of incoming and reflected-diffracted energy. In the synthetics, the first arrivals at the right flat port clearly show both a delay and a reduction of amplitude that indicates a shadow zone and, thus, diffraction. In Figure 6, the reflected P wave is clearly seen along the left canyon's wall. This wave precedes both reflected S and diffracted *creeping* Rayleigh waves that propagate along the canyon's surface. The creeping waves are produced at the corners and bounce back and forth between them. Early and late emissions of diffracted Rayleigh phases are clearly seen also in the flat part of the model.

Figure 7 shows that a deep canyon effectively acts as a barrier for surface waves. In this case, good agreement is found with the theoretical prediction of Fujii *et al.* (1984) for the amplitude of the reflected and transmitted Rayleigh waves at the corner of a quarter space. Such values are of about 30 and 68%,

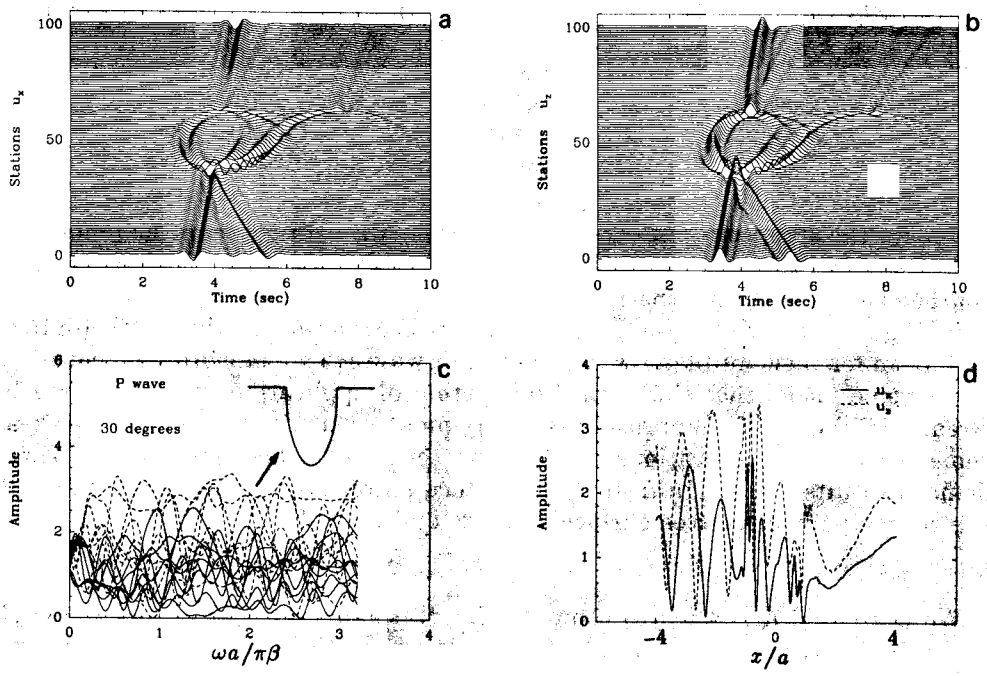

FIG. 6. Incidence of a plane P wave with incidence angle of 30°. Synthetic seismograms and frequency response for surface receivers equally spaced between $x = -4a$ and $x = 4a$ at the surface of a semi-elliptical canyon with maximum depth of $3a$. (a–d) Same as Figure 5.

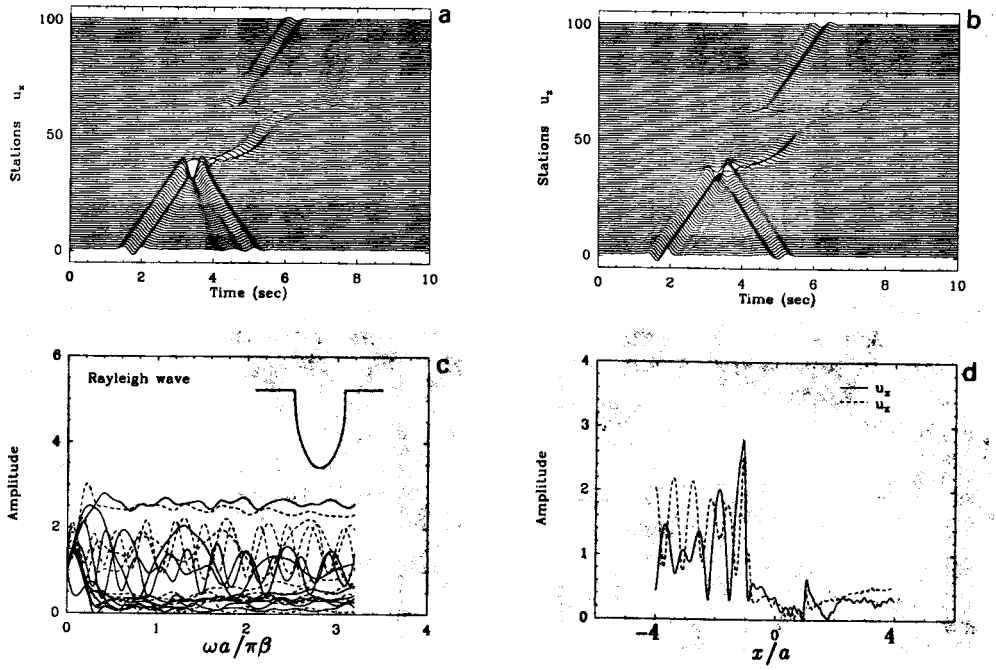

FIG. 7. Incidence of a plane Rayleigh wave. Synthetic seismograms and frequency response for surface receivers equally spaced between $x = -4a$ and $x = 4a$ at the surface of a semi-elliptical canyon with maximum depth of $3a$. (a-d) Same as Figure 5.

respectively. Amplification at the canyon's left rim are of about 2.5 for both components. Significant effects can be seen for the response of the left flat part.

The responses of the deep elliptical canyon to the two different types of incident waves show a common phenomenon, namely the appearance of creeping Rayleigh waves that produce the identical patterns on Figures 6 and 7.

Figure 8 corresponds to SV waves incident on a mountain with unit slopes. Top amplification in frequency domain reaches 4. However, maximum amplification for the other stations does not exceed the level of two times the amplitude of incident wave. Forward scattering of SV to Rayleigh waves is the salient characteristics of the synthetics.

In Figures 9 and 10, we present the surface motion of the semi-elliptical mountain for incident plane P and Rayleigh waves. This topographic feature is an extreme model that shows the wide potential applications of this approach. Great variability of amplifications in frequency domain is again present: at some receivers amplifications reach values of about 4 for the P wave. Time-domain results show significant interference patterns of creeping waves along the curved part of the free surface and late emission of Rayleigh waves.

CONCLUSIONS

We presented a method to compute the diffraction of P, SV, and Rayleigh waves by an irregular topographic feature in an elastic half-space. It is based on a direct integral representation of the diffracted elastic fields in terms of single layer boundary sources. A discretization scheme based on the numerical and analytical integration of exact Green's functions for displacements and tractions

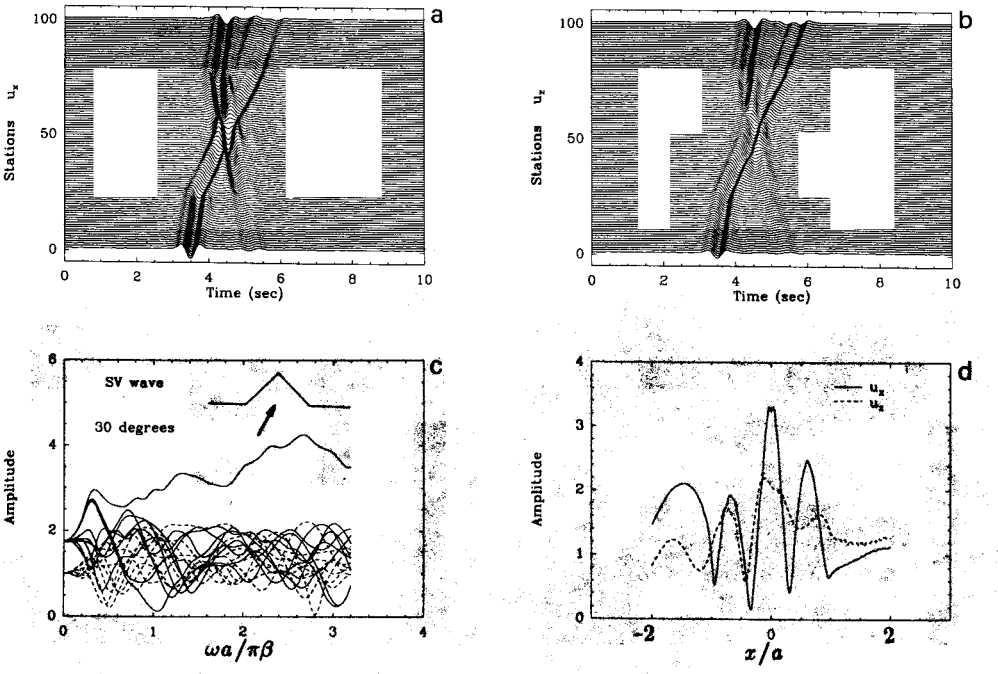

FIG. 8. Incidence of a plane SV wave with incidence angle of 30°. Synthetic seismograms and frequency response for surface receivers equally spaced between $x = -2a$ and $x = 2a$ at the surface of a triangular mountain with unit slopes. (a–d) Same as Figure 5.

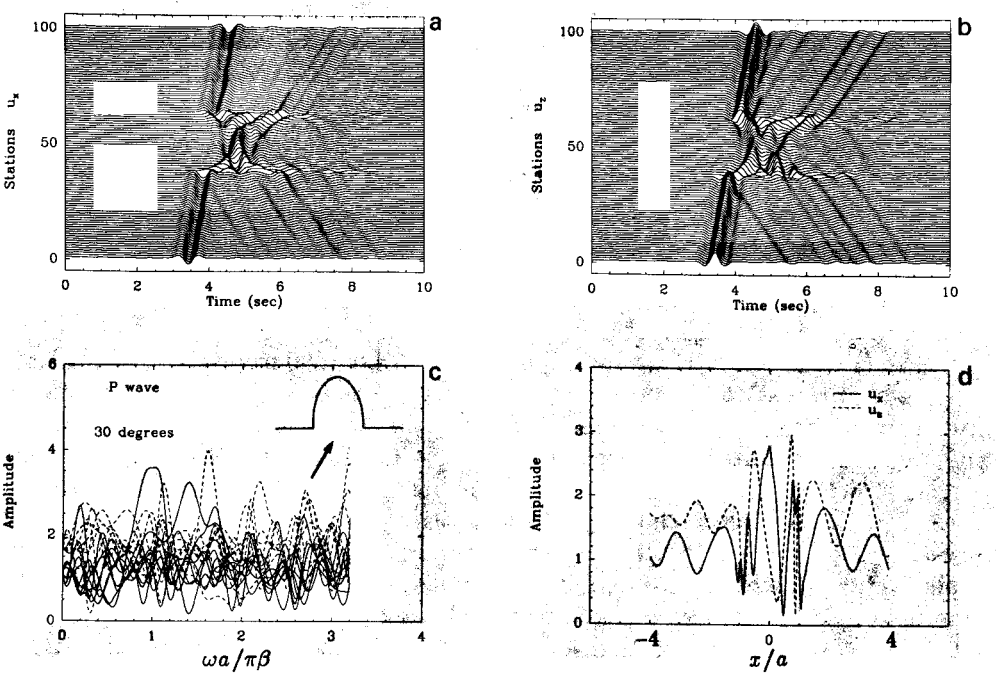

FIG. 9. Incidence of a plane P wave with incidence angle of 30°. Synthetic seismograms and frequency response for surface receivers equally spaced between $x = -4a$ and $x = 4a$ at the surface of a semi-elliptical mountain with maximum height of $2a$. (a–d) Same as Figure 5.

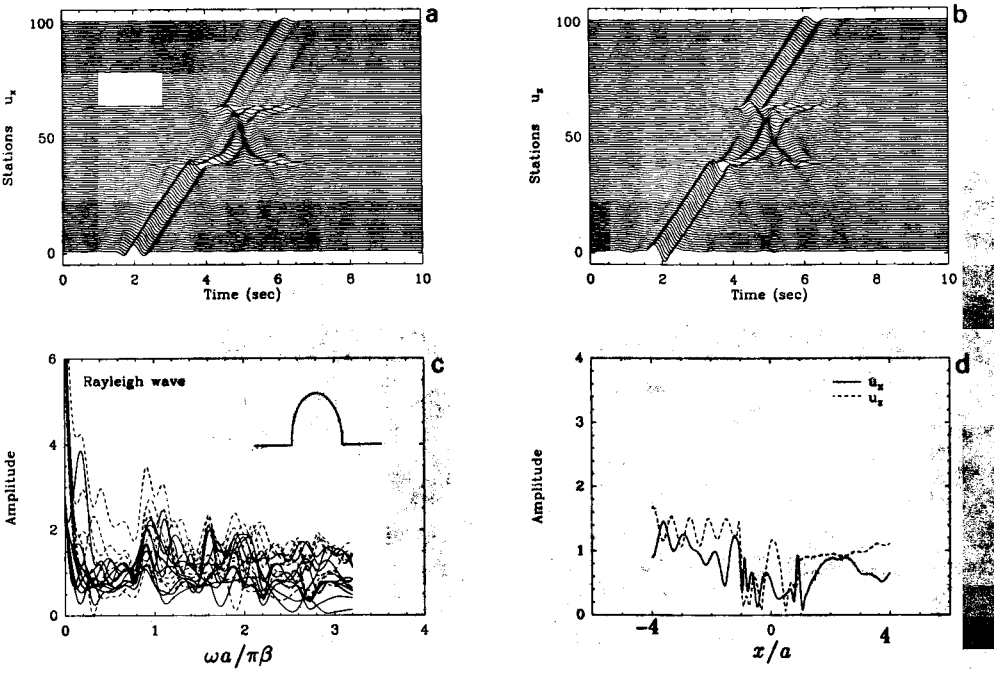

FIG. 10. Response to a nearby vertical load. Except at low frequencies, results correctly describe the effects of an incoming Rayleigh wave. Synthetic seismograms and frequency response for surface receivers equally spaced between $x = -4a$ and $x = 4a$ at the surface of a semi-elliptical mountain with maximum height of $2a$. (a–d) Same as Figure 5.

is employed. Our formulation can be seen as a numerical realization of Huygens' principle, i.e., the diffracted waves are constructed at the boundary from which they are radiated. Therefore, an advantage of the single-layer representation is that absorbing boundaries are not required. In addition to the physical insight gained with this method, it appears to be accurate and fast.

These results correspond to a relatively simple set of conditions, namely: (1) the incidence of a plane wave (or the application of a vertical load in the neighborhood), (2) the assumption of an elastic half-space with Poisson ratio of 1/4, and (3) symmetrical shape for the irregularity. Nevertheless, they display significant aspects of the response on topographic features. One of these is the spectacular amplitude of creeping waves and, as its counterpart, the large increase of duration of the motion on the irregular topography.

It is of interest to consider the plots of the frequency response at selected receivers. It has been commonplace in the literature on site effects to say, for instance, that results show large variability with respect to frequency, incidence angle, and location of receivers. Our results confirm that indeed such is the case. They show that variability is not restricted to the topographic feature. Its presence strongly affects nearby locations. This is more dramatic for elevated topographies in which a large duration coda may arise. They also show that the interaction of elastic waves produce complex amplification and deamplification patterns. We believe that, despite the relative simplicity of the models studied, our results give a glimpse of the effects that the real topographic feature may induce. They present very large relative amplifications values that can be in many cases larger than 10.

A direct look at the frequency response at various locations shows why the spectral ratio technique cannot account for the seismic behavior of topographies. In fact, the large variability of the spectral content of ground motion in both frequency and spatial domains may explain why the search for a simple "topographic factor" remains so far futile. In order to interpret the data, we cannot rule out the need of a quantitative model and careful assessment of the type of incoming waves as well. In any event, our results show that the absolute level of amplification is generally lower than about four times the amplitude of incoming waves.

Acknowledgments

Thanks are given to M. Bonnet for his comments and suggestions and to F. J. Chávez-García and V. Farra for the critical reading of the manuscript. K. Aki, P.-Y. Bard, M. Bouchon, V. Farra, G. Jobert, M. Koller, R. Madariaga, A. Tarantola, J. E. Vidale, and A. Wirgin made valuable suggestions. The critical comments from an unknown reviewer helped to improve this paper. This research was done while one of us (F.J.S.-S.) was on leave from the National University of Mexico and the Centro de Investigación Sísmica A. C., México, at the Université Joseph Fourier of Grenoble, France, and at the Laboratoire de Sismologie of the Institute de Physique du Globe of Paris, France, as a Visiting Professor. Some computations were performed at Centre de Calcul Vectoriel pour la Recherche. This work was partially supported by the Pole Grenoblois de Recherche sur les Risques Naturels, by University of Paris VI, France, and by the Departamento del Distrito Federal, México.

References

Abramowitz, M. and I. A. Stegun (1972). *Handbook of Mathematical Functions,* Dover, New York.

Achenbach, J. D. (1973). *Wave Propagation in Elastic Solids,* North-Holland, Amsterdam.

Aki, K. (1988). Local site effects on strong ground motion, in *Earthquake Engineering and Soil Dynamics II: Recent Advances in Ground Motion Evaluation,* J. L. Von Thun (Editor), Geotechnical Special Publication No. 20, Am. Soc. Civil Engr., New York, 103-155.

Aki, K. and K. L. Larner (1970). Surface motion of a layered medium having an irregular interface due to incident plane *SH* waves, *J. Geophys. Res.* **75,** 1921-1941.

Aki, K. and P. G. Richards (1980). *Quantitative Seismology,* W. H. Freeman, San Francisco.

Banerjee, P. K. and R. Butterfield (1981). *Boundary Element Methods in Engineering Science,* McGraw Hill, London.

Bard, P.-Y. (1982). Diffracted waves and displacement field over two-dimensional elevated topographies, *Geophys. J. R. Ast. Soc.* **71,** 731-760.

Bonnet, G. (1986a). *Méthode des Équations Intégrales Appliquée à la mécanique,* Université Joseph Fourier, Grenoble.

Bonnet, M. (1986b). Méthode des équations intégrales régularisées en élastodynamique, *Doctorate Thesis,* École Nationale des Ponts et Chaussées, Paris.

Bonnet, M. (1989). Regular boundary integral equations for three-dimensional finite or infinite bodies with and without curved cracks in elastodynamics, in *Boundary Element Techniques: Applications in Engineering,* C. A. Brebbia and N. G. Zamani (Editors), Computational Mechanics Publications, Southampton.

Bouchon, M. (1973). Effect of topography on surface motion, *Bull. Seism. Soc. Am.* **63,** 615-632.

Bouchon, M. (1985). A simple, complete numerical solution to the problem of diffraction of *SH* waves by an irregular surface, *J. Acoust. Soc. Am.* **77,** 1-5.

Bouchon, M., M. Campillo, and S. Gaffet (1989). A boundary integral equation-discrete wavenumber representation method to study wave propagation in multilayered media having irregular interfaces, *Geophysics* **54,** 1134-1140.

Bouden, M., K. R. Khair, and S. K. Datta (1990). Ground motion amplification by cylindrical valleys embedded in a layered medium, *Int. J. Earthq. Eng. Struct. Dyn.* **19,** 497-512.

Bravo, M. A., F. J. Sánchez-Sesma, and F. J. Chávez-García (1988). Ground motion on stratified alluvial deposits for incident *SH* waves, *Bull. Seism. Soc. Am.* **78,** 436-450.

Brebbia, C. A. (1978). *The boundary Element Method for Engineers,* Pentech Press, London.

Campillo, M. (1987). Modeling of *SH* wave propagation in an irregularly layered medium: application to seismic profiles near a dome, *Geophys. Prospect.* **35,** 236-249.

Campillo, M. and M. Bouchon (1985). Synthetic *SH* seismograms in a laterally varying medium by the discrete wavenumber method, *Geophys. J. R. Ast. Soc.* **83,** 307-317.

Campillo, M., F. J. Sánchez-Sesma, and K. Aki (1990). Influence of small lateral variations of a soft surficial layer on seismic ground motion, *Int. J. Soil Dyn. Earthquake Eng.* **9,** 284-287.

Coutant, O. (1989). Numerical study of the diffraction of elastic waves by fluid-filled cracks, *J. Geophys. Res.* **94,** 17805-17818.

Dravinski, M. (1982). Influence of interface depth upon strong ground motion, *Bull. Seism. Soc. Am.* **72,** 597-614.

Dravinski, M. and T. K. Mossessian (1987). Scattering of plane harmonic *P*, *SV*, and Rayleigh waves by dipping layers of arbitrary shape, *Bull. Seism. Soc. Am.* **77,** 212-235.

Eshraghi, H. and M. Dravinski (1989). Scattering of elastic waves by nonaxisymmetric three-dimensional dipping layer, *J. Num. Methods Partial Differential Equations* **5,** 327-345.

Fujii, K., S. Takeuchi, Y. Okano, and M. Nakano (1984). Rayleigh wave scattering at various wedge corners, *Bull Seism. Soc. Am.* **74,** 41-60.

Gaffet, S. and M. Bouchon (1989). Effects of two-dimensional topographies using the discrete wavenumber-boundary integral equation method in *P-SV* cases, *J. Acoust. Soc. Am.* **85,** 2277-2283.

Geli, L., P.-Y. Bard, and B. Jullien (1988). The effect of topography on earthquake ground motion: a review and new results, *Bull. Seism. Soc. Am.* **78,** 42-63.

Kawase, H. (1988). Time-domain response of a semicircular canyon for incident *SV*, *P*, and Rayleigh waves calculated by the discrete wavenumber boundary element method, *Bull. Seism. Soc. Am.* **78,** 1415-1437.

Kawase, H. and K. Aki (1989). A study on the response of a soft basin for incident *S*, *P*, and Rayleigh waves with special reference to the long duration observed in Mexico City, *Bull. Seism. Soc. Am.* **79,** 1361-1382.

Kawase, H. and K. Aki (1990). Topography effect at the critical *SV*-wave incidence: possible explanation of damage pattern by the Whittier Narrows, California, earthquake of 1 October 1987, *Bull. Seism. Soc. Am.* **80,** 1-22.

Khair, K. R., S. K. Datta, and A. H. Shah (1989). Amplification of obliquely incident seismic waves by cylindrical alluvial valleys of arbitrary cross-sectional shape. Part I. Incident *P* and *SV* waves, *Bull. Seism. Soc. Am.* **79,** 610-630.

Koush-Bille, L., F. J. Sánchez-Sesma, and A. Wirgin (1991). Response resonante d'une montagne cylindrique a une onde sismique *SH*, *C. R. Acad. Sci. Paris* **312,** Série II, 849-854.

Kummer, B., A. Behle, and F. Dorau (1987). Hybrid modeling of elastic wave propagation in two-dimensional laterally inhomogeneous media, *Geophysics* **52,** 765-771.

Kupradze, V. D. (1963). *Dynamical Problems in Elasticity,* in *Progress in Solid Mechanics,* vol. 3, I. N. Sneddon and R. Hill (Editors). North-Holland, Amsterdam.

Lamb, H. (1904). On the propagation of tremors over the surface of an elastic solid, *Philos Trans. Roy. Soc. Lond. Sec. A.* **203,** 1-42.

Love, A. E. H. (1944), *A Treatise on the Mathematical Theory of Elasticity,* Dover, New York.

Luco, J. E., H. L. Wong, and F. C. P. De Barros (1990). Three-dimensional response of a cylindrical canyon in a layered half-space, *Intl. J. Earthq. Eng. Struct. Dyn.* **19,** 799-817.

Sánchez-Sesma, F. J. (1978). Ground motion amplification due to canyon of arbitrary shape, *Proc. 2nd Intl. Conf. Microzonation,* **2,** 729-742.

Sánchez-Sesma, F. J. (1987). Site effects on strong ground motion, *Intl. J. Soil Dyn. Earthquake Eng.* **6,** 124-132.

Sánchez-Sesma, F. J. (1990). Elementary solutions for the response of a wedge-shaped medium to incident *SH* and *SV* waves, *Bull. Seism. Soc. Am.* **80,** 737-742.

Sánchez-Sesma, F. J., M. A. Bravo, and I. Herrera (1985). Surface motion of topographical irregularities for incident *P*, *SV*, and Rayleigh waves, *Bull. Seism. Soc. Am.* **75,** 263-269.

Sánchez-Sesma, F. J., M. Campillo, and K. Irikura (1989). A note on the Rayleigh hypothesis and the Aki-Larner method, *Bull. Seism. Soc. Am.* **79,** 1995-1999.

Sánchez-Sesma, F. J. and J. Esquivel (1979). Ground motion on alluvial valleys under incident plane *SH* waves, *Bull. Seism. Soc. Am.* **69,** 1107-1120.

Sánchez-Sesma, F. J. and E. Rosenblueth (1979). Ground motion at canyons of arbitrary shape under incident *SH* waves, *Intl. J. Earthq. Eng. Struct. Dyn.* **7**, 441–4450.

Trifunac, M. D. (1971). Surface motion of a semi-cylindrical alluvial valley for incident plane *SH* waves, *Bull. Seism. Soc. Am.* **61**, 1755–1770.

Trifunac, M. D. (1973), Scattering of plane *SH* waves by a semi-cylindrical canyon, *Intl. J. Earthquake Eng. Struct. Dyn.* **1**, 267–281.

Wong, H. L. (1979). Diffraction of *P*, *SV* and Rayleigh waves by surface topographies, Report CE 79-05, Dept. of Civil Engineering, University of Southern California, Los Angeles.

Wong, H. L. (1982). Effect of surface topography on the diffraction of *P*, *SV*; and Rayleigh waves, *Bull. Seism. Soc. Am.* **72**, 1167–1183.

Wong, H. L. and P. C. Jennings (1975). Effect of canyon topographies on strong ground motion, *Bull. Seism. Soc. Am.* **65**, 1239–1257.

Woods, R. D. (1968). Screening of surface waves in soils, *J. Soil Mech.*, Found Div. Am. Soc. Civil Engrs., **94**, 951–979.

Instituto de Ingeniería, UNAM
Ciudad Universitaria, Apdo, 70-472
Coyoacán 04510, México, D.F.
México
(F.J.S.-S.)

Centro de Investigación Sísmica, A.C.
Fundación J. Barros Sierra
Carr. al Ajusco 203, Col. H de Padierna
Tlalpán 14200, México D.F.
México
(F.J.S.-S.)

Observatoire de Grenoble
Université Joseph Fourier
L.G.I.T.-I.R.I.G.M.
B.P. 53X
38041 Grenoble Cedex
France
(M.C.)

Manuscript received 13 June 1990